DOI: 10.1177/0954410014544303

Journal name
000(00):1–13

DOI:doi number
http://mms.sagepub.com

A Methodology for Vehicle and Mission Level Comparison of More Electric Aircraft Subsystem Solutions - Application to the Flight Control Actuation System

Imon Chakraborty* **and Dimitri N. Mavris**†
Aerospace Systems Design Laboratory, Georgia Institute of Technology, Atlanta, GA 30332, USA

Mathias Emeneth‡ **and Alexander Schneegans**§
PACE America Inc., Seattle, WA 98115, USA

Abstract

As part of the More Electric Initiative, there is a significant interest in designing energy-optimized More Electric Aircraft, where electric power meets all non-propulsive power requirements. To achieve this goal, the aircraft subsystems must be analyzed much earlier than in the traditional design process. This means that the designer must be able to compare competing subsystem solutions with only limited knowledge regarding aircraft geometry and other design characteristics. The methodology presented in this work allows such tradeoffs to be performed, and is driven by subsystem requirements definition, component modeling and simulation, identification of critical or constraining flight conditions, and evaluation of competing architectures at the vehicle and mission level. The methodology is applied to the flight control actuation system, where electric control surface actuators are likely to replace conventional centralized hydraulics in future More Electric Aircraft. While the potential benefits of electric actuation are generally accepted, there is considerable debate regarding the most suitable electric actuator - electrohydrostatic or electromechanical. These two actuator types form the basis of the competing solutions analyzed in this work, which focuses on a small narrowbody aircraft such as the Boeing 737-800. The competing architectures are compared at both the vehicle and mission levels, using as metrics subsystem weight and mission fuel burn respectively. As shown in this work, the use of this methodology aids the decision-making process by allowing the designer to rapidly evaluate the significance of any performance advantage between the competing solutions.

Keywords

More Electric Aircraft, More Electric Initiative, electric actuator, electrohydrostatic actuator, electromechanical actuator

* Senior Graduate Researcher, Aerospace Systems Design Laboratory, School of Aerospace Engineering, Georgia Tech, Corresponding author; e-mail: imonchakraborty@gatech.edu
† Boeing Chaired Professor, School of Aerospace Engineering, and Director, Aerospace Systems Design Laboratory, Georgia Tech
‡ Senior Business Development Manager, PACE America
§ Founding Member, PACE GmbH, and President, PACE America

1. Introduction - Consideration of More Electric Subsystems in Conceptual Design

The conceptual design phase of the traditional aircraft design process typically gives only limited consideration to the aircraft subsystems[1], which are addressed mainly in the late-preliminary and detailed design phases (1). This approach has proven adequate when applied to aircraft with conventional subsystem solutions due to the presence of a continuously-updated historical database and a relative lack of coupling/interactions between different subsystems.

This will not be the case, however, for conceptual design of More Electric Aircraft (MEA) or, in the limit, All Electric Aircraft (AEA), for which there is no equivalent historical data, and where subsystem interactions may be significant. As indicated by Faleiro, MEA/AEA design will necessitate a new design paradigm that considers the aircraft and its subsystems as a system of systems (2). More thorough consideration must therefore be given to the requirements, interactions, and effects of the aircraft subsystems even in the conceptual design phase.

This paper presents a requirements-driven methodology aimed at MEA/AEA design that integrates the analysis of subsystem requirements and effects with the conceptual phase aircraft sizing process (Fig. 1(a)). For each subsystem, the functional requirements are set by identifying constraining operating scenarios. The subsystem is sized to those requirements using conceptual phase aircraft parameters from the aircraft sizing analysis (dimensions, estimated takeoff gross weights, etc.). Fallouts such as subsystem weight (W_{sub}), non-propulsive power requirement (P_{np}), and drag coefficient change (ΔC_D, if any), can be fed back to the aircraft and propulsion system sizing analyses for the subsequent iteration (if 'Cycle?= Yes'). The convergence of this iterative process yields a design where conceptual design parameters such as aircraft weight, wing area, propulsion requirements, etc. were computed by representing subsystem requirements and effects *explicitly*.

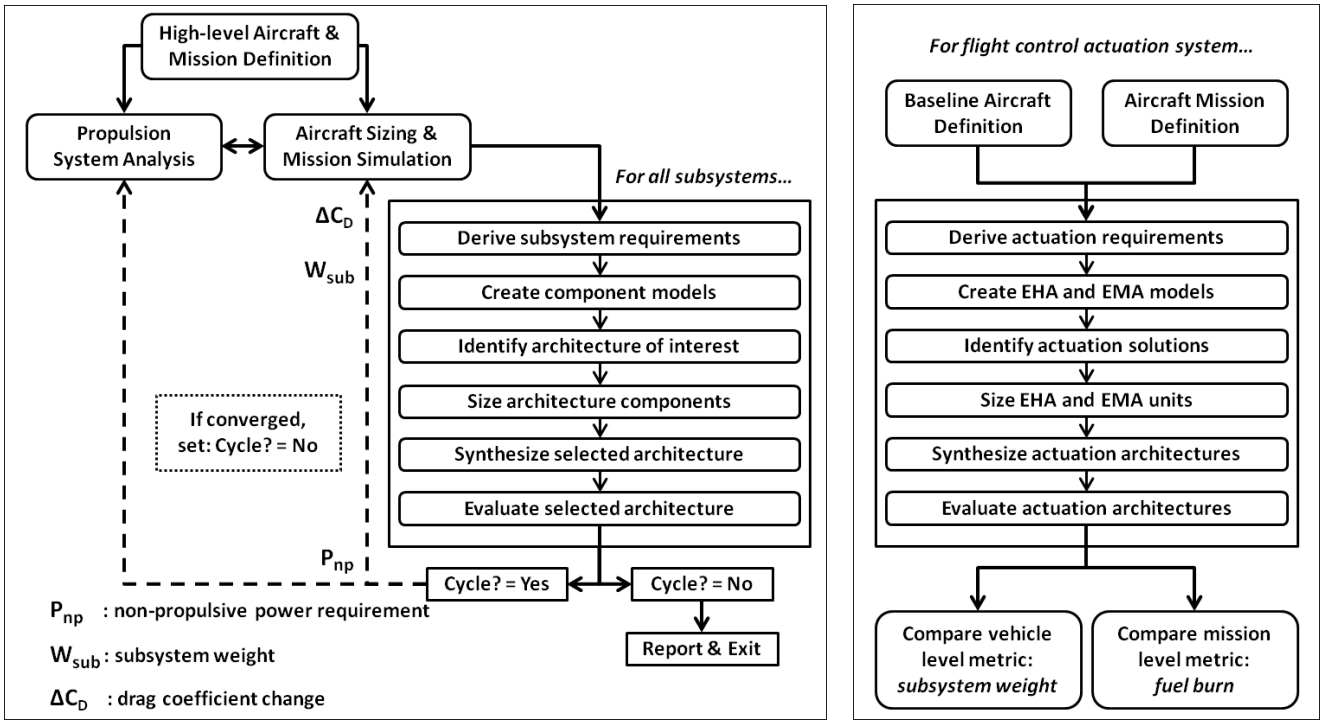

(a) Methodology linking subsystem sizing with traditional conceptual design phase aircraft sizing, with feed-back information flow to enable design "cycling" in response to subsystem changes

(b) Application to flight control actuation system with electrically actuated flight control surfaces

Fig. 1. Integrating subsystem sizing into the traditional aircraft sizing activity in the conceptual design phase

[1] In this work, by "subsystems" the authors mean Aircraft Equipment Systems (AES) such as actuation systems for flight control surfaces, landing gear, thrust reversers, nosewheel steering, and wheel braking, the environmental control system (ECS) and ice protection systems (IPS), engine starting, etc.

This paper focuses on the application of this methodology to electric flight control actuation systems. As seen in Fig. 1(b), the steps involved mirror the general steps of Fig. 1(a), and form the subject of subsequent sections of the paper. Section 2 gives an overview of flight control actuation systems. Section 3 derives the actuation requirements of the control surfaces, which feed into the actuator models that are described in Section 4. Section 5 identifies two configurations of interest and develops their corresponding architectures. Section 6 shows a comparison of the two configurations at the vehicle level, based on subsystem weight. Section 7 compares the two configurations at the mission level, based on fuel burn. Section 8 contains the conclusions drawn from this work and avenues identified by the authors for future work.

2. Overview of Flight Control Actuation Systems - Hydraulic vs. Electric

Most commercial and military aircraft in service today use centralized hydraulic systems for actuating flight control surfaces, landing gear, brakes, thrust reversers, etc. These systems, utilizing electric or engine-driven pumps to pressurize hydraulic fluid to 20 - 35 MPa (3,000 - 5,000 psi), have been matured through decades of aeronautical experience, with redundancy achieved through the incorporation of multiple physically segregated independent systems.

However, the inevitable technology saturation reached by hydraulics coupled with significant improvements in the power densities of power electronics and electric drives (3, 4) have led to a renewed interest in the research and development of electric actuators for flight control actuation as part of the More Electric Initiative (MEI). Compared to centralized hydraulics, electric actuators have the advantage of "Power on Demand", consuming power only when the control surface moves or overcomes a load. Moreover, they require only electrical energy input (Power By Wire) and allow the removal of bulky hydraulic lines, offering potential aircraft level weight savings. An additional advantage stems from the fact that electric actuators are Line Replaceable Units (LRUs), and are much easier to remove/install than hydraulic actuators.

The majority of research and development activities related to electric actuation has been on the military side, starting as far back as the 1950s with the British V-bombers (4). More recent efforts have been undertaken in the United States (5), involving the C-141 Starlifter (6), NASA's F-18 Systems Research Aircraft (7, 8), the AFTI F-16 (9), and most recently the F-35 Joint Strike Fighter (10). On the civil aviation side, a notable More Electric Aircraft (MEA) is the Airbus A380, where electric actuators are used in a backup role for certain control surfaces (11). This "2H/2E" configuration has been claimed to offer a 450 kg (1,000 lb) weight savings compared to a conventional "3H" configuration (12). With the exception of the Joint Strike Fighter, other flight test programs and analyses have focused on only single control surface types at a time, e.g. flaperon (7, 8), aileron (6), spoiler (13, 14), or high lift devices (15). In this work, since the entire flight control actuation system must be represented, all the aircraft flight control surfaces were considered simultaneously.

Electric actuator concepts fall mainly into two categories, within which there may be architectural variations - the electrohydrostatic actuator (EHA) and the electromechanical actuator (EMA). Each has advantages and disadvantages relative to the other, and there is significant debate (and no consensus) within the community regarding the type more applicable to flight control surface actuation. The EHA and EMA form the competing technologies analyzed in this work.

The competing subsystem *solutions* or *architectures* were formed by associating the competing technologies (EHA or EMA) to the aircraft control surfaces, a multitude of which are present even on small narrowbody aircraft. These associations were developed taking into consideration flight-criticality of the control surfaces, control surface redundancy, etc.

The current analysis utilized MATLAB/Simulink and Pacelab SysArc, an interactive system architecture investigation platform developed by PACE Aerospace Engineering and Information Technology GmbH[2]. It comprises a Knowledge Designer (KD) where system components (control surfaces, actuators, etc.) were mathematically modeled, and an Engineering Workbench (EWB), using which the configuration architectures were developed. For additional details regarding the use of Pacelab SysArc for aircraft architectural analysis, the interested reader is referred to Chakraborty et al. (16). The proposed methodology can of course be applied using other analysis tools as well.

[2] Organization website: www.pace.de Pacelab SysArc: www.pace.de/products/preliminary-design/pacelab-sysarc

3. Control Surface Actuation Requirements

Even for aircraft of similar size, the precise control surface configuration is often influenced by organizational design philosophy, especially for high-lift devices (17). To demonstrate this methodology, the control surface configuration and dimensions of the Boeing 737-800 aircraft were utilized. Each wing contains an outboard aileron and four flight spoilers for roll control. Aft elevators and a trimmable horizontal stabilizer (THS) provide pitch control, and a single rudder controls yaw. The high lift system comprises two inboard Krueger flaps, four outboard leading edge slats, and two double-slotted trailing edge flaps on each wing. The speedbrake function is performed by the symmetric deployment of all flight spoilers in the air, and is supplemented on the ground by the deployment of two ground spoiler panels on each wing.

For hinged control surfaces, the required actuation load can be characterized by the maximum hinge moment $M_{h,max}$. The hinge moments developed for the ailerons, elevator, and rudder may be expressed in standard form by

$$M_h = \bar{q}\, S_f\, c_f\, (C_{h,0} + C_{h,\alpha}(M)\, \alpha_{eff} + C_{h,\delta}(M,\delta)\, \delta), \tag{1}$$

where $\bar{q}$ is the dynamic pressure, M is the Mach number, α_{eff} is the effective angle of attack seen by the main surface, δ the control surface deflection, and S_f and c_f are the control surface planform area and chord. $C_{h,0}$, $C_{h,\alpha}$, and $C_{h,\delta}$ are hinge moment coefficients representing the effect of main lifting surface camber, α_{eff}, and δ on the hinge moment.

The hinge moment coefficients were determined based on the geometries of the control surfaces and associated main lifting surfaces using the empirical methodology of Roskam (18). Hinge moments predicted using these coefficients were validated against published hinge moments from flight tests of the NASA F-18 Systems Research Aircraft (7). This comparison, shown in Fig. 2, yielded acceptable agreement between predicted and observed hinge moments. For the flight and ground spoilers, the method proposed by Scholz (19) was used to determine hinge moment coefficients.

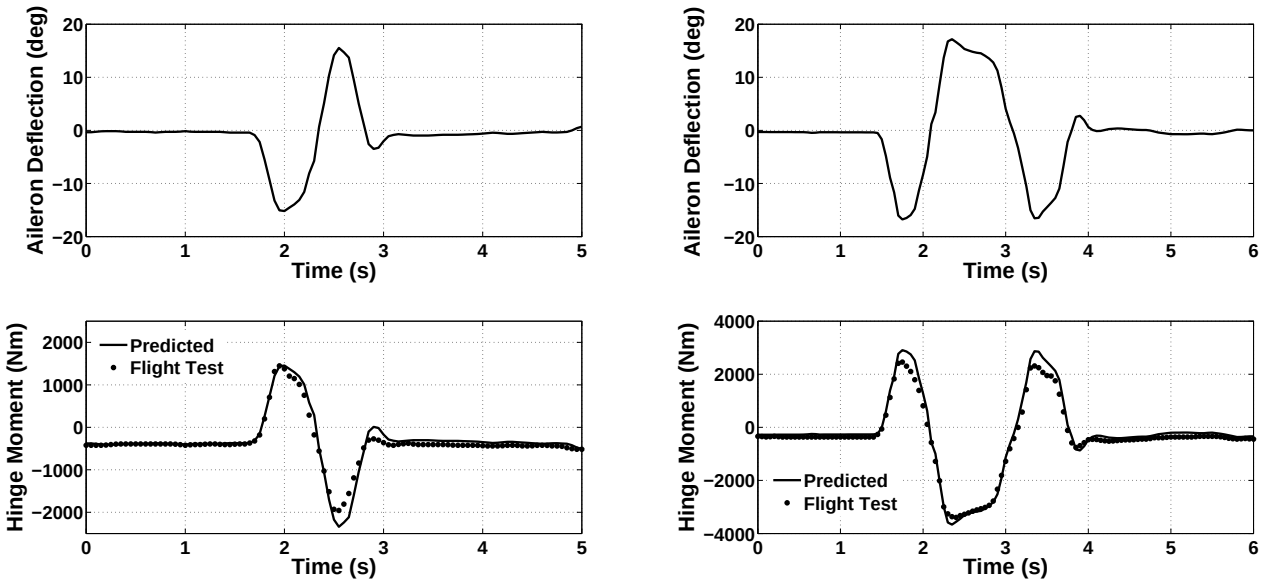

(a) Abrupt roll doublet - full stick (left): M = 0.72, h = 7,620 m (25,000 ft), q-bar = 13.60 kPa (284 lbf / ft^2)

(b) Abrupt aileron reversal - full stick (left): M = 0.84, h = 7,620 m (25,000 ft), q-bar = 18.29 kPa (382 lbf / ft^2)

Fig. 2. Comparison of hinge moments predicted using Roskam's method with flight test data from NASA's F-18 SRA

For each primary control surface, the flight condition (represented by $\bar{q}$, α_{eff}, and δ) that yields the maximum hinge moment can be obtained from the relevant Federation Aviation Regulations (FARs), and have been identified by Scholz (19).

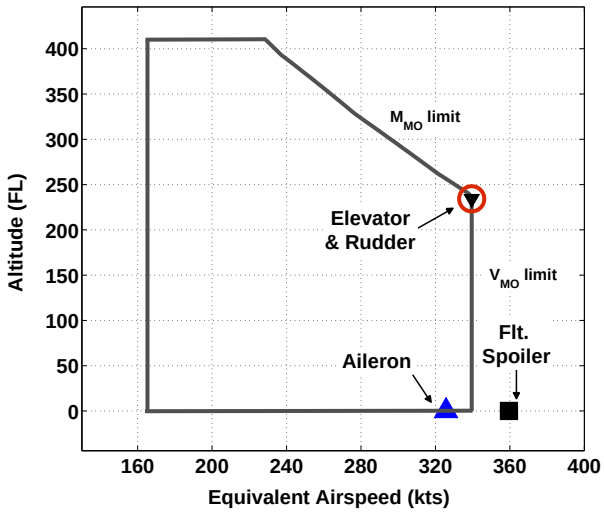

Fig. 3. Boeing 737-800 flight envelope with maximum hinge moment flight condition for ailerons, elevators, rudder, and flight spoilers

For the aileron, it is given by FAR 25.349, and corresponds to the maximum hinge moment from among three flight conditions - abrupt and full deflection at design manuever speed (V_A), a deflection yielding the same roll rate at design cruise speed (V_C), and a deflection yielding a third of the roll rate at the design dive speed (V_D). For the elevators, FAR 25.255 specifies the required positive and negative recovery load factors that must be available following a "runaway" failure of the THS. For the rudder, the applicable FARs are FAR 25.149 (one engine inoperative) and FAR 25.351 (permissible rudder deflections). FAR 25.351 and FAR 25.255 were evaluated over the aircraft altitude-speed envelope to determine the most critical flight condition yielding the maximum hinge moment (Fig. 3). For the flight spoilers, the maximum hinge moment occurs when they are extended during an emergency descent performed at the design dive speed (V_D). Since "weight-on-wheels" is required for ground spoiler deployment, the maximum rated tire speed was used to compute their actuation load requirement.

High lift device actuating loads strongly depend on flap mechanism kinematics, which vary significantly between both aircraft and manufacturers (17). In lieu of a detailed analysis of any one mechanism, the maximum actuation loads for the Krueger flaps and slats were derived using force and moment coefficients from published wind tunnel analyses (20, 21). For the trailing edge flaps, the required actuation load was set to the ratings of the existing leadscrew type actuators[3].

The maximum angular rates of ailerons, elevators, rudder, and flight spoilers were set based on the observed trend of higher rate requirements for modern automatic flight control systems (22). Representative rates for the high lift devices were obtained by timing videos of these devices deploying. Table 1 summarizes the derived actuation requirements.

Table 1. Summary of flight control surface actuation requirements for example small narrowbody aircraft

Control Surface	Actuating Load	Rate	#/aircraft
Ailerons	4,200 Nm	$60^\circ/s$	2
Elevators	7,600 Nm	$60^\circ/s$	2
Rudder	8,200 Nm	$60^\circ/s$	1
Flight spoilers	4,200 Nm	$60^\circ/s$	8
Ground spoilers	3,800 Nm	$40^\circ/s$	4
Trailing-edge flaps	51,000 N	102 mm/s	4
Leading-edge slats	6,300 N	60 mm/s	8
Krueger flaps	5,600 Nm	$16^\circ/s$	4

[3] Boeing 737 linear ballscrew flap actuator, Triumph Gear Systems, Triumph Group, Inc., High-Lift Actuation Systems product data-sheet. Available online: www.triumphgroup.com/companies/triumph-gear-systems-park-city/Documents, accessed Feb 25, 2014.

4. Electrohydrostatic and Electromechanical Actuator Models

Linear type actuators (as opposed to rotary actuators) were considered in this work. The relationship between control surface angular movement and actuator ram linear movement for hinged control surfaces is governed by the kinematics of the control surface to actuator linkage (Fig. 4(a)). This allows the actuator's output force F_L, ram speed v, and ram position x to be computed from the control surface's hinge moment, angular rate, and angular position.

The actuator is sized based on the required load-speed envelope, shown notionally in Fig. 4(b). Its stall load F_0, no-load (maximum) speed v_{max}, and stroke Δx_{max} can be computed from the maximum control surface hinge moment $M_{h,max}$, maximum angular rate $\dot{\delta}_{max}$, control surface angular range $\Delta\delta_{max}$, and the linkage kinematics (Fig. 4(a)).

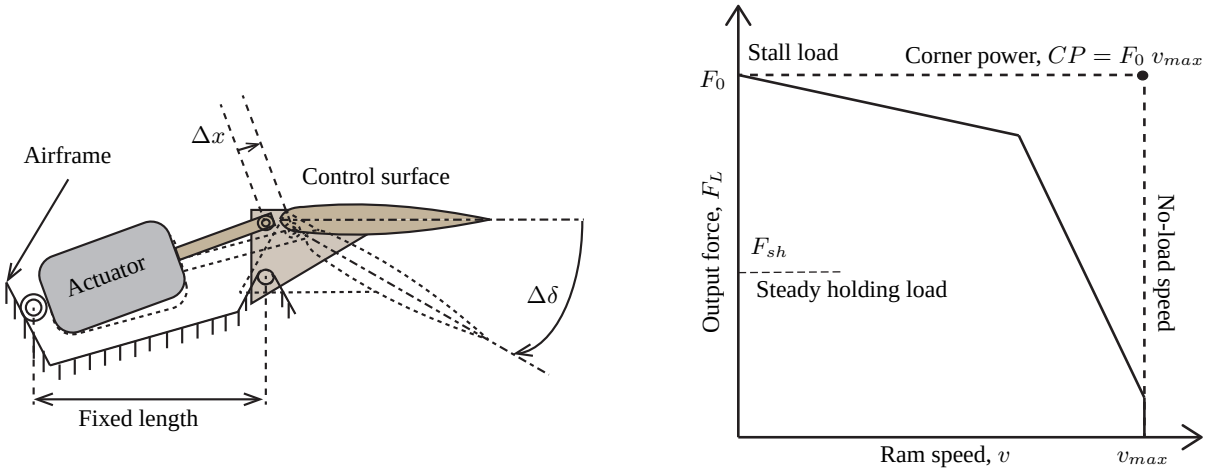

(a) Actuation of hinged control surface using linear actuator

(b) Actuator load vs. speed envelope

Fig. 4. Control surface linkage kinematics and actuator load-speed envelope

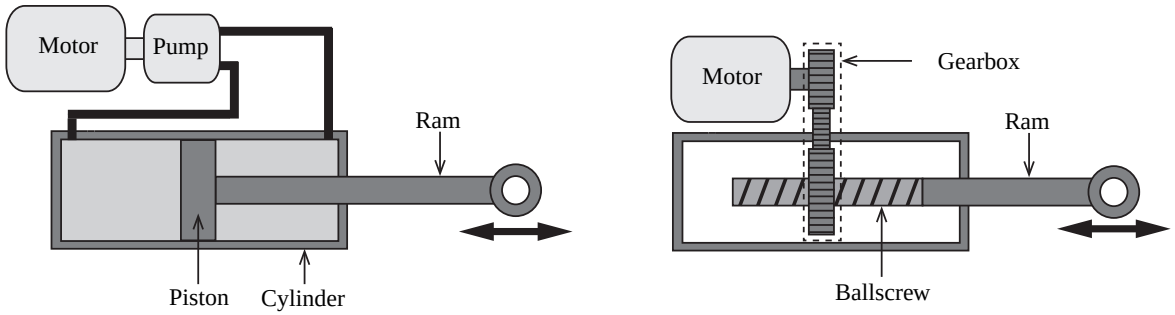

(a) Electrohydrostatic Actuator (EHA)

(b) Electromechanical Actuator (EMA)

Fig. 5. Notional schematic of electrohydrostatic and electromechanical actuators

4.1. Electrohydrostatic Actuator (EHA)

In the EHA, a bidirectional motor is directly mated to a bidirectional, fixed-displacement pump, which actuates a hydraulic cylinder whose piston is connected to the actuator output ram (Fig. 5(a)). The cylinder pressure difference Δp required to achieve an output force F_L, and a piston velocity $\dot{x}$ with acceleration $\ddot{x}$ is given by

$$\Delta p = \frac{1}{A_p}(m_r\ddot{x} + c\dot{x} + F_L), \tag{2}$$

where A_p is the piston cross-sectional area, m_r the mass of reciprocating components (piston + output rod + balance rod), and c the viscous friction coefficient. The required piston area was computed by evaluating Eq. 2 at the stall load condition and with maximum pressure difference, i.e., with $F_L = F_0, \dot{x} = \ddot{x} = 0, \Delta p = \Delta p_{max}$. Cylinder components were sized considering the loads applicable for each, e.g., piston rod diameter based on tension/compression and buckling, cylinder wall thickness based on tensile and circumferential (Hoop) stresses, etc (23). The cylinder mass m_c was computed by summing the computed masses of the constituent components and the enclosed hydraulic fluid, and considering the cylinder configuration (single or tandem).

The required total pump flow Q_{tot} is given by the sum of the ideal flow Q_i and the leakage flow Q_l, i.e.

$$Q_{tot} = Q_i + Q_l = A_p \dot{x} + c_{lkg} \Delta p, \tag{3}$$

where c_{lkg} is the leakage coefficient. The pump shaft speed ω_p and required shaft torque τ_p are given by

$$\omega_p = \frac{Q_{tot}}{D_{pump}}, \qquad \tau_p = \frac{\Delta p \, D_{pump}}{\eta_h}, \tag{4}$$

where D_{pump} is related to the pump displacement[4] as $D_{pump} = (\text{pump displacement})/(2\pi)$ and η_h is the pump efficiency. Since the leakage flow is typically much smaller than the ideal flow, the maximum flow rate corresponds to the maximum ram velocity, i.e. $Q_{tot}^{max} \approx A_p v_{max}$. For the EHA, the motor and pump shaft speeds and torques are physically identical, i.e. $\omega_m = \omega_p, \tau_m = \tau_p$. The required maximum speed and shaft torque of the motor are then given by

$$\omega_m^{max} = \frac{A_p v_{max}}{D_{pump}}, \qquad \tau_m^{max} = \frac{\Delta p_{max} \, D_{pump}}{\eta_h}. \tag{5}$$

A parametric pump model was used to compute the pump mass m_p based on the pump displacement. This included the mass of the hydraulic fluid present within the pump, while the mass of the hydraulic fluid in the lines connecting the pump to the cylinder was accounted for using the mass calibration factor discussed in a subsequent section.

4.2. Electromechanical Actuator (EMA)

In the EMA, a bidirectional motor drives a reduction gearbox which in turn drives a ballscrew that converts the rotational motion of the gearbox output shaft to the linear motion of the actuator output ram (Fig. 5(b)). The gearing ratios of the ballscrew and the gearbox were defined as

$$G_{bs} = \frac{\omega_{bs}}{v}, \qquad G_{gb} = \frac{\omega_m}{\omega_{bs}}, \tag{6}$$

where ω_{bs} is the angular speed of the rotating member of the ballscrew. The gearing ratios can be used to relate actuator no-load speed and stall load to maximum motor shaft speed and shaft torque:

$$\omega_m^{max} = v_{max} \, G_{bs} \, G_{gb}, \qquad \tau_m^{max} = \frac{F_0}{(\eta_{bs} \, G_{bs})(\eta_{gb} \, G_{gb})}, \tag{7}$$

where η_{bs} and η_{gb} are the ballscrew and gearbox efficiencies. For this work, a gearbox efficiency of $\eta_{gb} = 0.9$ was used. The ballscrew efficiency was computed as $\eta_{bs} = \tan \alpha_{bs} / \tan(\alpha_{bs} + \phi_{bs})$, where $\phi_{bs} = \tan^{-1} \mu_{bs}$ is the friction angle and $\alpha_{bs} = \tan^{-1}(1/(G_{bs} r_{bs}))$ is the screw helix angle. The radius of the screw r_{bs} was selected as the larger of the radius computed from buckling consideration and that from consideration of combined axial and torsional loading (23).

[4] Pump displacement is defined as the fluid volume pumped per unit revolution (mm^3/rev or in^3/rev).

For the gearbox, the number of stages required to attain the overall gearbox ratio G_{bs} was computed as $n = \text{ceil}\left(log(G_{gb})/log(G_{stg}^{max})\right)$, where $G_{stg}^{max} = 2L_{cc}/d_{min} - 1$ is the maximum stage reduction ratio for a given center-to-center distance L_{cc} and minimum permissible pinion diameter d_{min}. The gearbox mass m_{gb} was computed after determining the gear face width from strength considerations (23), and accounting for the number of driver-driven pairs.

4.3. Motor and Power Electronics

A brushless DC (BLDC) motor was considered for both the EHA and EMA cases, as this type of motor has been successfully flight-tested in electric actuators (8). Using parametric BLDC torque-speed characteristics (24), the required motor output torque (τ_{out}^{max}) was determined based on the following criteria:

1. The peak output torque given by Eq. 5 and Eq. 7 must be met with a torque margin applied to satisfy acceleration requirements against actuator inertia.
2. The actuator force-speed ($F - v$) envelope, when reduced to a torque-speed ($\tau - \omega$) envelope by the actuator gearing, must be contained within the motor torque-speed envelope.
3. The motor's maximum continuous torque must meet the actuator's steady-holding load requirement.

Evaluating the input electrical power over the boundary of the motor $\tau - \omega$ envelope (accounting for losses whose magnitudes depend on the operating point in the envelope), the maximum electrical input power P_{in}^{max} was determined. Torabzadeh-Tari (25) provides an empirical estimate of the mass of a BLDC motor based on τ_{out}^{max} and P_{in}^{max} as

$$m_{em} = 10^{-3} \left(\frac{4.7}{\tau_{out}^{max}}\right)^{-0.84} \left(1222 + 26.7\,(f_1 - 375)^{0.28} + 0.98\,(P_{in}^{max} - 491)^{0.11}\right) \quad [kg] \tag{8}$$

where f_1 is the source fundamental frequency. The same author also provides an estimate for the weight of the power electronics as

$$m_{pe} = 10^{-3} \left(\frac{400}{V_{in}^{AC}}\right)^{0.02} \left(2290 + 0.3\,(f_{sw} - 6000)^{0.8} + 0.3\,(P_{in} - 2000)^{1.1}\right) \quad [kg] \tag{9}$$

where f_{sw} is the switching frequency, V_{in}^{AC} is the input AC voltage (for this work, the actuators are powered from 135 VAC buses), and P_{in} is obtained by scaling the motor's maximum input power P_{in}^{max} by the assumed efficiency of the power electronics. For actuator designs comprising two motors, each was assumed to have its own power electronic unit.

4.4. Actuator Weight Computation

Since the component mass estimation described above accounts for only the major actuator components, but neglects other components such as fittings, clamps, etc., simply adding these masses would likely under-predict total actuator mass. To compensate, an additive (likely under-predicted) estimate of actuator mass was first obtained by adding the computed masses of the main components while factoring in the number of component units $N_{(.)}$ present in one actuator, i.e.

$$\begin{aligned} m_{EHA} &= m_c + N_p.m_p + N_{em}.m_{em} + N_{pe}.m_{pe} \\ m_{EMA} &= m_{bs} + N_{gb}.m_{gb} + N_{em}.m_{em} + N_{pe}.m_{pe} \end{aligned} \tag{10}$$

To determine the magnitude of the under-prediction, the masses predicted using Eq. 10 were compared against published masses of electric actuators available from previous analyses or flight tests. For each such case, the actuator was sized to the same stall load, no-load rate, and stroke as the published actuators. Additional information regarding the actuator layout

(such as electrohydraulic or electromechanical redundancy) was incorporated whenever available[5]. A calibration factor of 1.15 (i.e., + 15 %) applied to the predicted cylinder, pump, ballscrew, and gearbox masses produced reasonable agreement, as shown in Tables 2 and 3 for EHA and EMA respectively.

Table 2. Comparison of predicted vs. published EHA weight following calibration

Description	F-18 SRA flaperon	Typical tandem EHA
Source	Navarro (7)	Sadeghi & Lyons (26)
Stall load	59.16 kN (13,300 lbf)	142.34 kN (32,000 lbf)
No load rate	195.6 mm/s (7.7 in/s)	203.2 mm/s (8.0 in/s)
Stroke	114.3 mm (4.5 in)	-
Layout	1 3ϕ PMM $\rightarrow$ 1 FDP	Dual EH channel, 2 TC/surface
Published weight	18.8 kg (41.5 lb)	72.3 kg (159.5 lb)
Predicted weight	19.1 kg (42 lb)	74.4 kg (164 lb)

Table 3. Comparison of predicted vs. published EMA weight following calibration

Description	F-18 SRA flaperon	Transport spoiler	C-141 aileron
Source	Jensen et al. (8)	Fronista & Bradbury (14)	Thompson (6)
Stall load	58.72 kN (13,200 lbf)	222.4 kN (50,000 lbf)	84.74 kN (19,050 lbf)
No load rate	170.2 mm/s (6.7 in/s)	177.8 mm/s (7.0 in/s)	118.1 mm/s (4.65 in/s)
Stroke	104.8 mm (4.125 in)	152.4 mm (6.0 in)	137.9 mm (5.43 in)
Layout	2 3ϕ BLDCM $\rightarrow$ 1 BS	1 5ϕ SRM $\rightarrow$ 1 BS	2 M/GB $\rightarrow$ 1 BS
Published weight	11.8 kg (26 lb)	17.7 kg (39 lb)	15.9 kg (35 lb)
Predicted weight	11.8 kg (26 lb)	18.1 kg (40 lb)	16.8 kg (37 lb)

5. Electric Flight Control Actuation System Architectures

The EHA and the EMA have certain advantages and disadvantages relative to the other, which is the cause of the EHA vs. EMA debate within the flight control actuation community.

If designed to the same stall load, no-load rate, and stroke, the EMA will generally be lighter than the EHA. This is seen in Fig. 6, which compares weight-optimal EHA and EMA designs for a range of hinge moments. The weight advantage of the EMA is seen to grow with the magnitude of the sizing hinge moment. The EMA is also potentially more energy-efficient as it converts electical power directly to mechanical power without an intermediate step of hydraulic/fluidic power.

However, with regard to flight control surface actuation, a critical hazard for the EMA is the possibility of certain single-point jam failures (27). Since a mechanical jam is involved, it is not possible to use multiple EMAs per control surface to provide redundancy either. This has caused some to question the EMA's suitability for actuating at least the flight-critical control surfaces, for which a control surface jam can be catastrophic and must be demonstrated to be less probable than 10^{-9} per hour (one occurrence for every billion flight hours).

Considering this same criterion, the EHA enjoys a major advantage in that it can be designed to be fail-safe. If a failure occurs, the hydraulic cylinder can be designed to enter a damped/bypass mode, preventing the actuator's output ram from jamming but simultaneously providing damping against flutter. This means that EHAs can be used in parallel to meet the 10^{-9} failure probability criterion, and are therefore applicable to flight-critical control surfaces. They can also be integrated with centralized hydraulics (e.g., Electrical Backup Hydraulic Actuator (EBHA) on Airbus A380 (11)).

The EMA may, however, be suitable for the actuation of flight and ground spoilers. Since these are not flight-critical control surfaces (their operation is not necessary for the continued safe flight of the aircraft), less stringent failure probability

[5] Abbreviations: 3ϕ - three phase, PMM - permanent magnet machine, FDP - fixed displacement pump, EH - electrohydraulic, TC - tandem cylinder, BLDCM - brushless DC motor, BS - ballscrew, SRM - switched reluctance machine, M/P - motor/pump, M/GB - motor/gearbox.

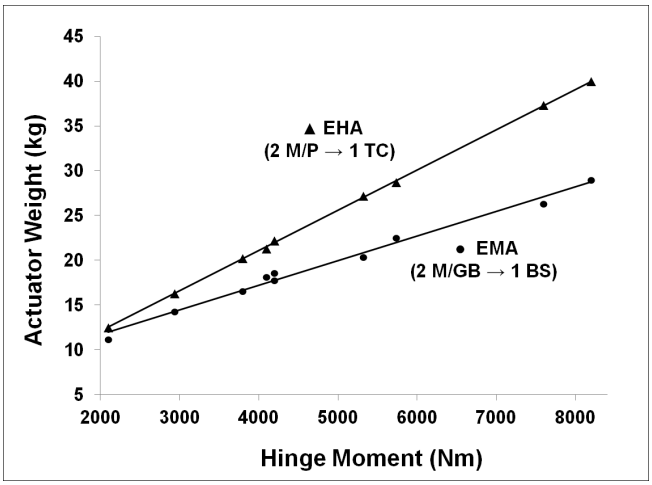

Fig. 6. Weight-optimal EHA and EMA designs vs. sizing hinge moment

requirements are applicable. In fact, EMA design for spoiler actuation was analyzed by Fronista and Bradbury (14) and Atallah et al. (13). A similar argument holds for the high lift devices, and an EMA-driven high lift system was analyzed experimentally and from a safety/reliability standpoint by Bennett et al. (15, 28). In line with this reasoning, the two control surface actuation configurations shown in Fig. 7 were selected for further analysis.

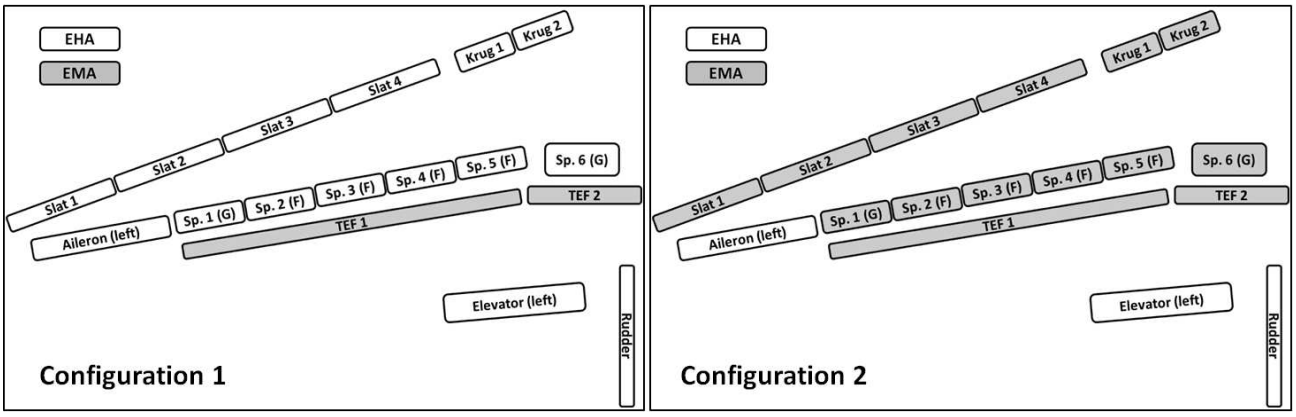

Fig. 7. *Configuration 1:* T/E flaps actuated by EMA-LS. All other surfaces actuated by EHA. *Configuration 2:* Ailerons, elevators, rudder actuated by EHA. L/E slats, Krueger flaps, and spoilers actuated by EMA. T/E flaps actuated by EMA-LS.

- Configuration 1: Other than the trailing-edge flaps (TEFs), all control surfaces are driven by EHAs. Two parallel EHAs are used to drive each aileron and elevator, while three are used for the rudder. Slats, Krueger flaps, flight spoilers, and ground spoilers are driven by a single EHA. Each trailing-edge flap is driven by two parallel Electromechanically Actuated Leadscrews (EMA-LS[6]).
- Configuration 2: The slats, Krueger flaps, flight spoilers, and ground spoilers are each actuated using a single EMA. Actuation for the remaining control surfaces is identical to Configuration 1.

A detailed functional hazard analysis was beyond the scope of the current work, but design practices from Boeing (29) and Airbus (30) were adopted to determine the nature of redundancy incorporated into the two architectures.

[6] EMA-LS: Electromechanically Actuated Leadscrew. A variant of the EMA in which the nut is the translating member instead of the rotating member. This is similar to the leadscrews used in the conventional Boeing 737-800 trailing edge flap system.

1. The stringent reliability requirements of the flight-critical primary control surfaces was met using a combination of *actuator redundancy* and *internal redundancy* (31). Actuator redundancy was provided by using two parallel actuators in active-active configuration for the elevators and ailerons, and three parallel actuators in active-active-standby configuration for the rudder. Only EHAs were considered for these surfaces due to their fail-safe characteristics, and parallel EHAs were powered from different electric buses. Each EHA driving a flight-critical control surface was assumed to have internal redundancy, in which two motor-pump pairs drove a tandem cylinder (2 M/P $\rightarrow$ 1 TC).
2. For non flight-critical control surfaces such as spoilers, slats, and Krueger flaps, *surface redundancy* already existed since there were multiple panels per wing. In this case, each panel was powered by a single actuator (either EHA or EMA). The actuators were connected to the electric buses in a way that ensured symmetric availability of control surfaces following the failure of any one bus.
3. Trailing edge flap panel were provided *actuator redundancy*, and were driven by two EMA-LS units at the two extremities (in practice, this also prevents panel warping due to aerodynamic loads), powered from different buses. Each EMA-LS had *internal redundancy* (6), in which two motor-gearbox pairs drove a ballscrew through a summing element.

6. Vehicle Level Analysis

For the two configurations shown in Fig. 7, a gradient-based constrained optimizaton was performed to obtain the weight-optimal EHA and EMA designs for the relevant control surfaces. For the EHA, maximum pump pressure and pump displacement were used as design variables, while for the EMA, the ballscrew and gearbox gearing ratios were used. For the EHA, there is an iterative loop between available pressure difference, cylinder sizing (and mass), and required pressure difference. A constraint was therefore enforced to ensure that the required pressure difference did not exceed the pump's maximum pressure difference. For the EMA, the ballscrew RPM was limited to a maximum permissible value (14). For both EHA and EMA, maximum limits were enforced for motor RPM and permissible current under stall load.

Table 4 shows the weight breakdown of the two architectures, which includes the weight of all weight-optimal actuators and also the associated wiring from the main electrical buses to the actuators. The wiring weight was computed by physically positioning the actuators in Pacelab SysArc, and then invoking the tool's routing algorithm. This algorithm converts logical connections between components (e.g., between a bus and an actuator) to physical equivalents, using connecting elements (electric wiring). Wire gauge is determined from voltage drop and current considerations, and length is determined based on user-defined allowable "pathways", though which electrical wiring is constrained to run.

Configuration 2 enjoys a weight advantage of 5.87 % over Configuration 1, but it should be noted that this weight advantage would be only 0.11 % of the Maximum Takeoff Weight (MTOW) of the Boeing 737-800 (79,000 kg).

Table 4. Weight comparison between Configuration 1 and Configuration 2

Control surface Actuators			**Config. 1 Weight (kg)**			**Config. 2 Weight (kg)**		
Name	#	Act./surf.	Design	Unit	Group	Design	Unit	Group
Aileron	2	2	EHA	15.8	63.2	EHA	15.8	63.2
Elevator	2	2	EHA	25.6	102.4	EHA	25.6	102.4
Rudder	1	3	EHA	27.0	81.0	EHA	27.0	81.0
Flight spoiler	8	1	EHA	10.2	81.6	EMA	9.0	72.0
Ground spoiler	4	1	EHA	8.4	33.6	EMA	8.9	35.6
Krueger flap	4	1	EHA	19.9	79.6	EMA	13.4	53.6
LE slat	8	1	EHA	16.3	130.4	EMA	9.7	77.6
TE flap	4	2	EMA-LS	44.5	356.0	EMA-LS	44.5	356.0
Total Weight of Actuators $\rightarrow$			Total $\rightarrow$		**927.8**	Total $\rightarrow$		**841.4**
Electrical Wiring			Len.(m)	AWG	Wt.(kg)	Len.(m)	AWG	Wt.(kg)
			571	4/0	544	571	4/0	544
Total Architecture Weight $\rightarrow$			Total $\rightarrow$		**1471.8**	Total $\rightarrow$		**1385.4**

7. Mission Level Analysis

Both configurations were evaluated over the course of the representative mission shown in Fig. 8. Primary control surface movements depend on the phase of flight (Table 5), and during the mission simulation, these were characterized using the normalized magnitudes of deflection in one or both directions and the cycles per second parameter which represents the frequency of movement (32). The high lift devices were assumed to deploy or retract in a manner consistent with what is observed in a typical commercial aircraft flight.

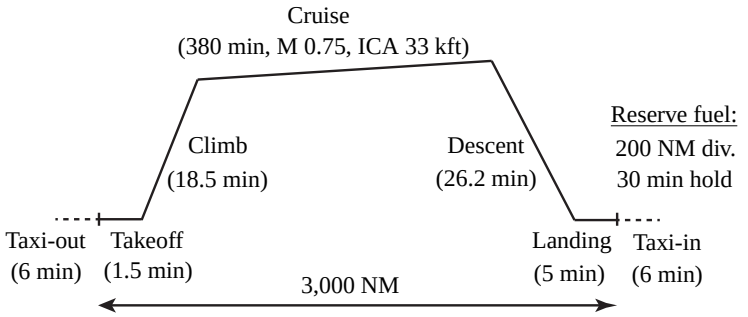

Fig. 8. Representative flight profile for mission level analysis. In addition to the 3,000 NM (380 min) flight shown, shorter flights of 350 NM (63 min), 850 NM (132 min), and 1,350 NM (202 min) were also evaluated.

Table 5. Characterization of aileron, elevator, rudder, and flight spoiler movements

Control →	Aileron		Elevator		Rudder		Flt. Spoiler	
Motion →	$+\bar{\delta}$/$-\bar{\delta}$	cps	$+\bar{\delta}$/$-\bar{\delta}$	cps	$+\bar{\delta}$/$-\bar{\delta}$	cps	$\bar{\delta}$	cps
Ground	+1/-1	0.4	+1/-1	0.4	+1/-1	0.4	1	0.4
Takeoff	+0.12/-0.2	0.4	+0.2/-0.2	0.4	+0.2/-0.2	0.4	0.12	0.4
Climb	+0.12/-0.2	0.2	+0.2/-0.2	0.2	+0.2/-0.2	0.2	0.12	0.2
Cruise	+0.5/-0.5	0.4	+0.3/-0.3	0.4	+0.3/-0.3	0.4	0.5	0.4
Descent	+0.12/-0.2	0.3	+0.2/-0.2	0.3	+0.2/-0.2	0.3	0.12	0.3
Landing	+0.4/-0.53	0.3	+0.53/-0.53	0.3	+0.53/-0.53	0.3	0.4	0.3

To compute the power consumed at the bus by the electric actuator, the control surface hinge moment and angular rate were converted to the required force (F_{req}) and speed (v_{req}) at the control/actuator linkage using the control surface gearing G_{cs}. These were then propagated through the mathematical model of the actuator to get the required torque (τ_{req}) and shaft speed ($\omega_{m,req}$) of the electric motor, effectively using the overall actuator gearing (G_{act}). The motor torque and shaft speed requirements were then evaluated in conjunction with the assumed torque-speed characteristics of the BLDC motor (24) to find the motor input power requirement. Finally, this was scaled using the assumed power electronics efficiency η_{pe} to give the power draw at the bus[7]. This is shown in Eq. 11 for a single-channel actuator.

$$M_h, \omega \xrightarrow{G_{cs}} F_{req}, v_{req} \xrightarrow{G_{act}} \tau_{req}, \omega_{m,req} \xrightarrow{\eta_{em}(\tau,\omega)} P_{in}^{em} \xrightarrow{\eta_{pe}} P_{in}^{pe} = P_{bus} \tag{11}$$

Certain control surface motions (e.g., flap deployment/retraction) occur only during a fraction of the duration of a mission segment. For these, the *average* power consumption over the duration of the mission segment $\bar{P}_{seg}$ was computed

[7] An alternate method is to estimate the power requirement at the control surface, i.e. the product of hinge moment and angular rate, and then scale successively by the efficiencies of all actuator components encountered to obtain the power draw at the bus. However, this method will predict zero power draw from the bus if the control surface is held *fixed* against a non-zero load, while in reality electric actuators are known to consume power in this condition. The method described above and used in this analysis does not suffer from this discrepancy.

using the mean power consumed during the motion $\bar{P}$ and the *activity ratio* ν as follows:

$$\nu = \frac{\Delta t_{active}}{\Delta t_{seg}} \in [0,1], \quad \Longrightarrow \quad \bar{P}_{seg} = \bar{P}\,\nu + 0.(1-\nu) = \bar{P}\,\nu. \tag{12}$$

As only the flight control actuation subsystem was being considered, the non-propulsive power requirements of the other subsystems (Table 6) were assumed to be identical for both configurations. The Environmental Control System (ECS) was assumed to have a bleedless architecture, and engine bleed air was used only for the cowl ice protection system (IPS), similar to the Boeing 787 arrangement. The power and bleed air demands of these systems were reported by Tagge et al. (33) for a Boeing 767-type airplane, and were scaled using guidelines reported by Cleveland (34) to Boeing 737-800 size. Power demands for instrumentation, communication, navigation (tabulated as 'instruments'), equipment and furnishings, lights, pumping fuel, and miscellaneous loads were also set in a similar manner. The power demand for the assumed electrical wing de-icing system was estimated using a rapid-evaluation method developed by Meier and Scholz (35) which was shown to have good agreement with the Boeing 787 wing IPS power demand. Centralized hydraulics were assumed to be retained to actuate the landing gear, landing gear bay doors, brakes, nosewheel steering, and cargo doors. The power consumption for these users for different flight phases was reported by de Tenorio (36) for the case of the similar-sized Airbus A320, and has been incorporated as a shaft-power offtake (to run engine-driven hydraulic pumps) in this work.

Table 6. Non-propulsive power requirements (excluding flight control actuation)

System	Type	Unit	Ground	Takeoff	Climb	Cruise	Descent	Landing	OEI
ECS	Bleedless	kVA	129	129	210	210	210	129	204
Instruments	Electric	kVA	8	8	8	8	8	8	8
Equipment	Electric	kVA	60	60	60	65	0	0	0
Fuel	EMDP	kVA	7.5	7.5	7.5	7.5	7.5	7.5	7.5
"	EDP	kW	7.5	7.5	7.5	7.5	7.5	7.5	7.5
Wing IPS	Electric	kVA	17	17	25	25	25	17	17
Cowl IPS	Bleed air	kg/s	2.2	2.2	0	0	2.2	2.2	1.1
Lights	Electric	kVA	10	10	10	10	10	10	10
Hyd. users	EDP	kW	1.43	0	0.67	0	0.44	9.83	9.83
Misc.	Electric	kVA	5	5	5	5	5	5	5
Demand	Electric	kVA	124	124	171	173	139	92	260
per	Mechanical	kW	4.9	4.1	4.5	4.1	4.4	9.5	15.2
Engine	Bleed	kg/s	1.1	1.1	0	0	1.1	1.1	1.1

The propulsion system characteristics were generated using the Environmental Design Space (EDS) tool (37) developed for the U.S. Federal Aviation Administration's Office of Environment and Energy (FAA/AEE) and NASA. At the core of this tool is the Numerical Propulsion System Simulation (NPSS) (38) tool, which was used to generate an engine deck that is representative of the CFM56-7B27 engine, but does not utilize or contain any proprietary information.

The difference between the two configurations in terms of mission fuel burn may be caused by a difference in either the non-propulsive power requirement or the subsystem weight. While both effects were considered in this work, the magnitude of the first was quite small, as seen from Table 7. Further, the peak power demand for flight control actuation (a factor influencing generator sizing) does not occur for any of the flight conditions of Table 7. Tagge et al. (33) note that this critical peak power flight condition is generally the one-engine inoperative (OEI) crosswind landing condition, where the combination of high load and rate requirements justifies a conservative sizing approach based on corner power[8]. Referring to Table 1 and assuming operability of both ailerons, both elevators, the rudder, and four out of eight flight spoilers in the OEI condition, the combined corner power evaluates to around 51 kW for *both* configurations.

[8] Corner power for a control surface is the product of maximum hinge moment and maximum angular rate.

Table 7. Flight control actuation power requirements for Configurations 1 and 2 (averaged over mission segment duration)

Segment	Configuration 1 (kW)			Configuration 2 (kW)		
	PFCS	SFCS	Total	PFCS	SFCS	Total
Ground	0.02	1.19	1.21	0.02	1.20	1.22
Takeoff	0.24	0.22	0.46	0.23	0.25	0.48
Climb	0.67	0.55	1.22	0.67	0.59	1.26
Cruise	0.99	-	0.99	0.98	-	0.98
(Turbulence)	4.96	-	4.96	4.92	-	4.92
Descent	0.97	0.54	1.51	0.96	0.57	1.53
Landing	3.26	0.22	3.48	3.24	0.26	3.50

Table 8. Mission fuel-burn comparison (Config. 2 relative to Config. 1)

Trip Distance $\rightarrow$	350 NM	850 NM	1,350 NM	3,000 NM
Block fuel Δ	- 0.06 %	- 0.08 %	- 0.09 %	- 0.11 %

The difference in mission fuel burn is primarily driven by the difference in weight between the two configurations (Table 4). In addition to the 3,000 NM mission shown in Fig. 8, the fuel burn differences were also evaluated over several intermediate trip distances more commonly encountered in small narrowbody aircraft operations, and are shown in Table 8.

8. Conclusions and Future Work

Motivated by the need to consider More Electric Aircraft (MEA) or All Electric Aircraft (AEA) subsystems in greater detail in the conceptual design phase, a methodology was presented that integrates the analysis of subsystem requirements and effects with the conceptual stage aircraft sizing process.

This requirements-driven methodology analyzes and sizes the subsystems based on functional requirements in conjunction with aircraft design parameters that are either available or easily estimable in the conceptual design phase. Since information regarding subsystem characteristics can be fed back into the aircraft and propulsion system sizing process, the converged design point obtained from this iterative scheme is one where the effect of aircraft characteristics on the subsystems and the feed-back effect of subsystem characteristics on aircraft and propulsor sizing have been accounted for explicitly. Such a methodology will give the conceptual phase designer of MEA/AEA the ability to rapidly evaluate the aircraft and mission level effects of subsystem architectures, allowing the subsystem concept space to be explored more thoroughly. The designer will therefore be able to make more informed decisions regarding subsystem architectures before progressing to the subsequent design phases, where design freedom is progressively reduced as configuration characteristics are “frozen”, and after which major design changes become expensive in terms of both time and cost.

The methodology was applied to the conceptual design phase analysis of the flight control actuation system of a small narrowbody aircraft (e.g., Boeing 737 or Airbus A320). Rather than comparing the effect of transitioning from hydraulic to electric flight control actuation systems, this paper compared two candidate electric actuation solutions. It was found that a configuration that employed electrohydrostatic actuators (EHAs) for flight-critical control surfaces and electromechanical actuators (EMAs) for non flight-critical ones enjoyed a marginal aircraft-level weight advantage over another predominantly-EHA configuration. A concomitant fuel burn advantage, driven primarily by the weight advantage, was also detected. The conceptual phase designer exercising this methodology would be in a position to weigh the observed advantages against additional considerations such as safety/reliability. In this specific case, considering the possibility of a single-point jamming failure of an EMA and the potentially hazardous flight conditions that may result from a jammed spoiler or high-lift device, the designer may be inclined to accept the marginal weight penalty of the predominantly-EHA configuration in exchange for its fail-safe nature.

Based on the experience and results obtained from this work, the authors have identified two main avenues for further research, which will be the subjects of future publications. The first avenue of research will be aimed at determining how the relative performance of the two actuation configurations varies as aircraft gross weight increases. In other words, how significant would the weight difference be if, instead of a Boeing 737 or Airbus A320-sized aircraft, a Boeing 747-sized or Airbus A380-sized aircraft is considered? As seen from Fig. 6, the magnitude of the EMA's weight advantage over the EHA increases as the actuation load increases. However, not only do larger-sized aircraft have larger overall control surface *planform areas*, they also generally have multiple control surface *sections* (e.g., a split rudder, or multiple aileron sections per wing). The actuators driving these split surfaces would be sized to smaller loads, but they would be larger in number. Second, some aircraft may have control surfaces such as inboard high-speed ailerons (e.g. Boeing 747) that others do not (e.g., Boeing 737). Thus instead of attempting to scale the results (which would disregard or mask these configurational differences), future work will attempt to "bound" the problem by assessing the two configurations applied to a small number of aircraft which taken together encompass a broad range of aircraft gross weights.

The second avenue of research will consider other aircraft subsystems such as the environmental control system (ECS), ice protection systems (IPS), etc. in addition to the flight control actuation system, using the same requirements-driven subsystem sizing methods discussed in this work. This will allow the conceptual designer to set mission requirements (payload, range, etc.) and compare a spectrum of aircraft subsystem architectures. For example, at the two extremes might be an AEA and another candidate with conventional subsystem architecture, with several MEA options in between. More Electric subsystem solutions applied to multiple subsystems may in this case result in large differences in the non-propulsive power requirements and weights of subsystems relative to a baseline with conventional architecture. In this case, the "feedback loop" of the proposed methodology will allow the "snowballing" effects of the subsystem changes on the overall aircraft characteristics to be captured. Depending on the case at hand, the difference in aircraft characteristics between "uncycled" (feedback loop not active) and "cycled" (feedback loop active) designs may be quite substantial, and something of considerable interest to the conceptual phase designer.

Acknowledgments

The authors would like to thank Mr. Christopher Perullo, Research Engineer II at the Aerospace Systems Design Laboratory, for supporting their investigation on the propulsion side with his expertise and experience with the EDS and NPSS tools.

Funding

This research received no specific grant from any funding agency in the public, commercial, or not-for-profit sectors.

References

[1] Raymer, D., *Aircraft Design: A Conceptual Approach*, AIAA Education Series, 4th ed.

[2] Faleiro, L., "Beyond the More Electric Aircraft," *AIAA Aerospace America*, 2005.

[3] Cronin, M., "The all-electric aircraft," *IEE Review*, Vol. 36, No. 8, sep 1990, pp. 309 –311.

[4] Jones, R., "The More Electric Aircraft - Assessing the Benefits," *Proceedings of the Institution of Mechanical Engineers, Part G, Journal of Aerospace Engineering*, Vol. 216, 2002, pp. 259–270.

[5] Cloyd, J., "Status of the United States Air Force's More Electric Aircraft initiative," *Aerospace and Electronic Systems Magazine, IEEE*, Vol. 13, No. 4, April 1998, pp. 17–22.

[6] Thompson, K., "Notes on 'The electric control of large aeroplanes'," *Aerospace and Electronic Systems Magazine, IEEE*, Vol. 3, No. 12, dec. 1988, pp. 19 –24.

[7] Navarro, R., "Performance of an Electro-Hydrostatic Actuator on the F-18 Systems Research Aircraft," *16th Digital Avionics Systems Conference, Irvine, California*, October 1997.

[8] Jensen, S., Jenney, G., and Dawson, D., "Flight test experience with an electromechanical actuator on the F-18 Systems Research Aircraft," *19th Digital Avionics Systems Conference, 2000*, Vol. 1, 2000, pp. 2E3/1 – 2E310.

[9] Burkhard, A. and Dietrich, R., "Joint Strike Fighter Integrated Subsystems Technology, A Demonstration for Industry, by Industry," *Journal of Aircraft*, Vol. 40, 2003, pp. 906–913.

[10] Vohnout, S., Bodden, D., Kim, B., Wagoner, R., Kunst, N., Edwards, P., Gleeson, B., Cascio, D., Brzuszkiewicz, S., Wagemans, R., Rounds, M., and Clements, N., "Prognostic-Enabling of an Electrohydrostatic Actuator (EHA) System," *Annual Conference of Prognostics and Health Management Society*, 2012.

[11] Van den Bossche, D., "The A380 Flight Control Electrohydrostatic Actuators, Achievements and Lessons Learnt," *25th International Congress of the Aeronautical Sciences, ICAS 2006*, 2006.

[12] Kulshreshtha, A. and Charrier, J., "Electric Actuation for Flight and Engine Control: Evolution and Challenges," *SAE-ACGSC Meeting 99*, SAE, Feb 28 - Mar 2 2007.

[13] Atallah, K., Caparrelli, F., Bingham, C., Schofield, N., Howe, D., Mellor, P., Maxwell, C., Moorhouse, D., and Whitley, C., "Permanent magnet brushless drives for aircraft flight control surface actuation," *Electrical Machines and Systems for the More Electric Aircraft (Ref. No. 1999/180), IEE Colloquium on*, 1999, pp. 8/1 –8/5.

[14] Fronista, G. and Bradbury, G., "An electromechanical actuator for a transport aircraft spoiler surface," *Energy Conversion Engineering Conference, 1997. IECEC-97., Proceedings of the 32nd Intersociety*, Vol. 1, 1997, pp. 694–698 vol.1.

[15] Bennett, J., Mecrow, B., Jack, A., and Atkinson, D., "A Prototype Electrical Actuator for Aircraft Flaps," *Industry Applications, IEEE Transactions on*, Vol. 46, No. 3, 2010, pp. 915–921.

[16] Chakraborty, I., Mavris, D., Emeneth, M., and Schneegans, A., "A System and Mission Level Analysis of Electrically Actuated Flight Control Surfaces using Pacelab SysArc," *AIAA Science and Technology Forum and Exposition (SciTech 2014)*, National Harbor, MD, January 13-17 2014.

[17] Rudolph, P., "High Lift Systems on Subsonic Commercial Airliners," NASA Contractor Report 4746 CONTRACT A46374D(LAS), National Aeronautics and Space Administration, September 1996 1996.

[18] Roskam, J., *Airplane Design Part VI - Preliminary Calculation of Aerodynamic, Thrust and Power Characteristics*, Design Analysis & Research, 1999.

[19] Scholz, D., "Development of a CAE-Tool for the Design of Flight Control and Hydraulic Systems," *AeroTech '95, Birmingham,*, 1995.

[20] Moraris, V., Lawson, N., and Garry, K., "Aerodynamic and Performance Characteristics of a Passive Leading Edge Krueger Flap at Low Reynolds Numbers," *The Aeronautical Journal*, Vol. 116 (1181), 2012, pp. 759–769.

[21] Kelly, J. and McCullough, G., "Aerodynamic Loads on a Leading-edge Flap and a Leading-edge Slat on the NACA 64A010 Airfoil Section (NACA TN 3220)," Tech. rep., National Advisory Committee for Aeronautics (NACA), 1954.

[22] Charrier, J. and Kulshreshtha, "Electric Actuation for Flight and Engine Control System: Evolution, Current Trends and Future Challenges," *45th AIAA Aerospace Sciences Meeting and Exhibit*, No. AIAA 2007-1391, Reno, Nevada, January 2007.

[23] Khurmi, R. and Gupta, J., *A Textbook of Machine Design*, Eurasia Publishing House (Pvt.) Ltd., 2005.

[24] Frischemeier, S., "Electrohydrostatic actuators for aircraft primary flight control - types, modelling and evaluation," *5th Scandinavian International Conference on Fluid Power, SICFP 1997, Linkoping, Sweden*, May 1997.

[25] Torabzadeh-Tari, M., *Dimensioning Tools of MEA Actuator Systems, Including Modeling, Analysis and Technology Comparison*, Ph.D. thesis, KTH Electrical Engineering, 2008.

[26] Sadeghi, T. and Lyons, A., "Fault Tolerant EHA Architectures," *IEEE AES Systems Magazine*, March 1992, pp. 32–42.

[27] Botten, S., Whitley, C., and King, A., "Flight Control Actuation Technology for Next-Generation All-Electric Aircraft," *Technology Review Journal - Millenium Issue*, 2000, pp. 55–68.

[28] Bennett, J., Mecrow, B., Atkinson, D., and Atkinson, G., "Safety-critical design of electromechanical actuation systems in commercial aircraft," *Electric Power Applications, IET*, Vol. 5, No. 1, 2011, pp. 37–47.

[29] Yeh, Y., "Triple-triple redundant 777 primary flight computer," *Aerospace Applications Conference, 1996. Proceedings., 1996 IEEE*, Vol. 1, feb 1996, pp. 293 –307 vol.1.

[30] Traverse, P., Lacaze, I., and Souyris, J., "Airbus Fly-by-Wire: A Process Towards Total Dependability," *ICAS 2006, 25th International Congress of the Aeronautical Sciences*, 2006.

[31] Bennett, J., Mecrow, B., Atkinson, D., and Atkinson, G., "Failure mechanisms and design considerations for fault tolerant aerospace drives," *Electrical Machines (ICEM), 2010 XIX International Conference on*, 2010, pp. 1–6.

[32] Simsic, C., "Electric actuation system duty cycles," *Aerospace and Electronics Conference, 1991. NAECON 1991., Proceedings of the IEEE 1991 National*, 1991, pp. 540–545 vol.2.

[33] Tagge, G., Irish, L., and Bailey, A. R., "Systems Study for an Integrated Digital/Electric Aircraft (IDEA)." *NASA Contractor Report 3840*, January 1985.

[34] Cleveland, F., "Size Effects in Conventional Aircraft Design," *Journal of Aircraft*, Vol. 7, No. 6, Nov-Dec 1970, pp. 483–512.

[35] Meier, O. and Scholz, D., "A Handbook Method for the Estimation of Power Requirements for Electrical De-Icing Systems," *DLRK, Hamburg*, Aug. 31 - Sept. 2 2010.

[36] de Tenorio, C., *Method for Collaborative Conceptual Design of Aircraft Power Architectures*, Ph.D. thesis, Georgia Institute of Technology, Atlanta, GA, USA, 2010.

[37] Kirby, M. and Mavris, D., "The Environmental Design Space," *26th International Congress of the Aeronautical Sciences (ICAS)*, Anchorage, Alaska, September 14-19 2008.

[38] "Numerical Propulsion System Simulation (NPSS): An Award Winning Propulsion System Simulation Tool," Online: https://www.grc.nasa.gov/WWW/RT/RT2001/9000/9400naiman.html.